

High-Resolution Regional Modeling of Urban Moisture Island: Mechanisms and Implications on Thermal Comfort

<https://doi.org/10.1016/j.buildenv.2021.108542>

Correspondence to Dr. J Song (HKU)

Abstract

The urban moisture island (UMI) can aggravate the thermal stress due to the urban heat island (UHI) in subtropical and tropical cities. In this study, we investigated the spatiotemporal variation patterns of UMI in Hong Kong, a subtropical coastal city, using the fine-resolution mesoscale Weather Research and Forecasting (WRF) model by integrating local climate zone (LCZ) maps based on the World Urban Database and Access Portal Tools (WUDAPT). Our results show that at regional scale, the UMI phenomenon tends to occur in coastal areas, possibly owing to rich moisture sources from sea breeze and inhibited moisture penetration due to barrier effects of mountains. Specifically, an all-day UMI effect was found in coastal low-density low-rise areas (LCZ5&8&10), while a nocturnal UMI effect and a daytime urban dry island (UDI) effect were found in coastal high-density high-rise areas (LCZ1&2). The UDI effect at daytime can be attributed to strong vertical moisture convection associated with intensive surface sensible heat fluxes in a strongly mixed urban boundary layer (UBL). The UMI effect at night can be attributed to blocked ventilation aisle, inhibited dewfall due to UHI, and weakened upward motion in a stable UBL. On the other hand, UMI can increase regional heat risks with additional 37.5% neighbourhoods in Extreme caution level and additional 6.1% neighbourhoods in Danger level. In addition, the impact of UMI on human thermal stress was found to be dominant at daytime in coastal low-density low-rise areas (LCZ5&8&10) and at nighttime in coastal high-density high-rise areas (LCZ1&2).

Keywords: urban moisture island, WRF simulation, thermal stress, local climate zone, WUDAPT

1. Introduction

Recent decades have seen rapid global urbanization associated with significant modifications on the land surface processes, which have significant implications on urban climate due to modulated surface heat and moisture balances [1-3]. One of the widely recognized urban climatic changes is the urban heat island (UHI) effect, e.g., the higher surface and air temperature in urban areas compared to the surrounding rural areas [4]. Another important but less-explored urban climatic change is the urban moisture island (UMI) effect, e.g., the higher humidity phenomena in urban areas. UHI and UMI effects in combination may result in a tremendous impact on public health in subtropical and tropical cities [5-7], especially during heatwave events [8-12]. High temperature can lead to severe thermal stress by restraining the heat dissipation of human bodies via thermal radiation and convection. On the other hand, high humidity can aggravate thermal stress by inhibiting sweating and skin evaporation. Extreme high temperature [8-11] and high humidity [12-15] were significantly associated with high mortality as well as the high hospitalization rate for infectious diseases, cardiovascular diseases, and respiratory diseases [5].

Therefore, unraveling the mechanisms of UHI and UMI is important to tackle the challenges caused by extreme weather. The UHI effect has been quite intensively studied over past decades [16, 17]. However, the UMI effect has not been widely recognized and lacks in-depth exploration. Some researchers found that the UMI phenomenon often occurred on clear and calm summer nights in littoral cities of temperate climate zones, such as Chicago [18], Krefeld [19], Vancouver [20] and London [21]. However, another subtropical coastal

compact high-rise city, Hong Kong, has reported an all-day UMI phenomenon [22]. Previous UMI studies usually focused on statistical analyses of the urban-rural humidity differences using point-scale observation data, with studies on UMI mechanisms and physical modeling of the UMI effect still rare. In particular, it is unclear about the impact of regional climates and urban forms on the UMI phenomenon.

The objective of this study is to explore the mechanism of the unique UMI phenomenon in Hong Kong by investigating spatiotemporal variations of air humidity through high-resolution regional climate modeling. Hong Kong is a typical subtropical city with unique mountainous terrains and compact urban morphology in limited developable coastal land areas. Most compact high-rise built-up areas are located within the relatively flat littoral belts, while most suburban and rural areas are surrounded by the inland mountains [23, 24]. Under the impact of the prevailing southerly background wind in summer, the moist sea breeze first penetrates and humidifies the compact urban areas, then climbs over mountains with mountain barrier effect at the leeward side, and finally enters inland suburban/rural areas, resulting in evident spatiotemporal differences of air humidity. In addition, intra-urban heterogeneity of air humidity can also be found due to different urban surface characteristics in different local climate zones (LCZs).

To better capture regional variation and intra-urban heterogeneity of air humidity and predict neighborhood-scale thermal stress, we first collected a high-resolution LCZ map of Hong Kong from World Urban Database and Access Portal Tools (WUDAPT) and integrated it into a multi-layer Weather

Research and Forecasting (WRF) model. The coupled WRF-WUDAPT model was applied over a typical heat wave event (23-28 June 2016) [25] so that the health implication of UMI can be considered. Specifically, research questions of the present study include: (1) simulate spatiotemporal variations in air humidity over Hong Kong (2) identify regional and intra-urban moisture transport mechanisms (3) investigate the aggravating impact of UMI on thermal stress. The current outcome will enhance our understanding of the urban climate in global subtropical and tropical cities, and contribute to the mitigation of UHI and UMI in these areas.

2. Model Configurations

2.1 Study area

The high-density, high-rise city of Hong Kong is located on China's southern coast between 22°08' N to 22°35' N, and 113°49' E to 114°31' E, embracing a typical subtropical and Asian monsoon climate with southwesterly and northeasterly prevailing wind directions in summer and winter, respectively. The summer is hot and wet with the monthly maximum temperature range of 30~35 °C and the monthly maximum humidity range of 81~83%. The winter is warm and humid with the monthly maximum temperature range of 18~21 °C and the monthly maximum humidity range of 70~79%. The total land area of Hong Kong is about 1064 km², including 75% hilly and rugged areas with Tai Mo Shan being the territory's highest point (957 m above sea level), and 25% flat areas consisting of 18.5% natural land and 6.5% manmade land reclaimed from the sea. As a result of the limited developable space and large population

(7.24 million in 2014), 95% of residents live in less than 20% of the total land area, among which most compact areas are concentrated in the littoral zones of Kowloon Peninsula and Hong Kong Island along the Victoria harbor.

2.2 Land-use dataset

To achieve a more accurate prediction of urban microclimate, high-resolution land use land cover (LULC) datasets with specific classifications of urban form and function are strongly needed, especially for rapidly expanding cities and city groups. Under this context, the World Urban Database Access Portal Tools (WUDAPT) project aims at acquiring urban morphology and LULC data for climate research. One of the first steps of the project is to map urbanized landscapes using local climate zones (LCZs) classification scheme [26]. The LCZ classification scheme categorizes LULC into 17 types based on surface morphology and material properties, 10 of which are urban (LCZ1-10) and the remaining 7 are natural (LCZ A-G). In this study, we collected the LCZ map of Hong Kong (Figure 1) from WUDAPT platform and found that [23] the dominant urbanized LCZ types include 54.8% Open High Rise (LCZ4), 24.6% Open Mid-rise (LCZ5) and 8.7% Compact High-rise (LCZ1). Urban morphological and thermal parameters in different LCZs are obtained from Stewart et al. [27] and Zheng et al. [24], before being ingested in WRF as described in section 2.3.

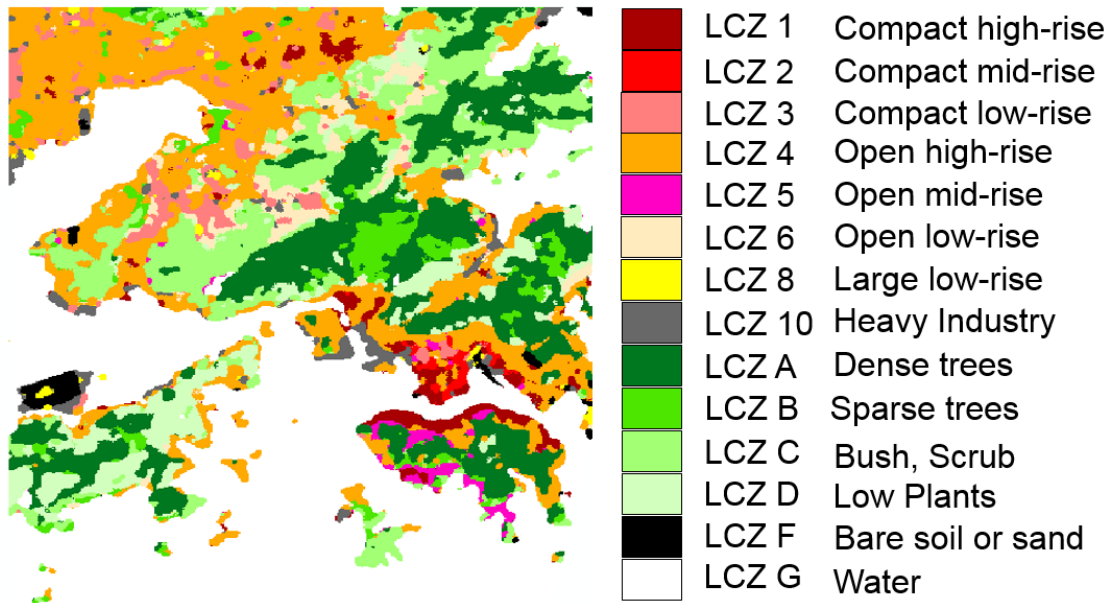


Figure 1. Map of local climate zones over Hong Kong.

2.3 Model configuration

To investigate the regional moisture transport mechanism and intra-urban variability of UMI intensity over Hong Kong, we integrated the above-mentioned high-resolution LCZ map into an advanced Weather Research and Forecasting (WRF) model (ARW version 3.6.1) [28]. A nested grid configuration with 5 one-way domains was constructed (Figure 2), with a resolution of 27 km (190×190), 9 km (238×239), 3 km (151×151), 1 km (151×151), and 0.333 km (241×181) for domains 1-5, respectively. In default settings, Moderate Resolution Imaging Spectroradiometer (MODIS) global land cover data (30-s) [29] were used in all 5 domains. To better capture the intra-urban heterogeneity, the MODIS dataset covering urban portions in the innermost domain (d05, Figure 2) was replaced by urban LCZ dataset using the method described in Martilli et al. [30]. To better capture urban land-atmosphere interactions in the vertical grid, 51 Eta levels were applied from the ground surface up to the top level of 50 hPa, with a fine resolution of 10 m in the urban canopy. The global reanalysis data from the

European Centre for Medium-Range Weather Forecasts (ECMWF) ERA-Interim with a resolution of $0.75^\circ \times 0.75^\circ$ was utilized as the initial and boundary meteorological conditions. Specifically, to investigate the impact of UMI on extreme heat risks, the large-scale meteorological data from 21 to 28 June in 2016 were used to drive the WRF model, with the first 40 hours from 21 to 22 June as the spin-up period and 5-day heat wave event (June 23-28, 2016) with relatively stable synoptic patterns [25, 31] as the analysis period.

Table 1 shows the physical parameterization schemes chosen in the present study [32, 33]. To better consider the two-way energy exchanges between the outdoor atmosphere and buildings equipped with air-conditioning systems, the multi-layer building effect parameterization-building energy model (BEP/BEM) [34, 35] was employed in this study. The target indoor air temperature and humidity as well as operation schedules of air-conditioning systems were set according to the parameter from the official document of Building Environmental Assessment Method (BEAM) of Hong Kong [36].

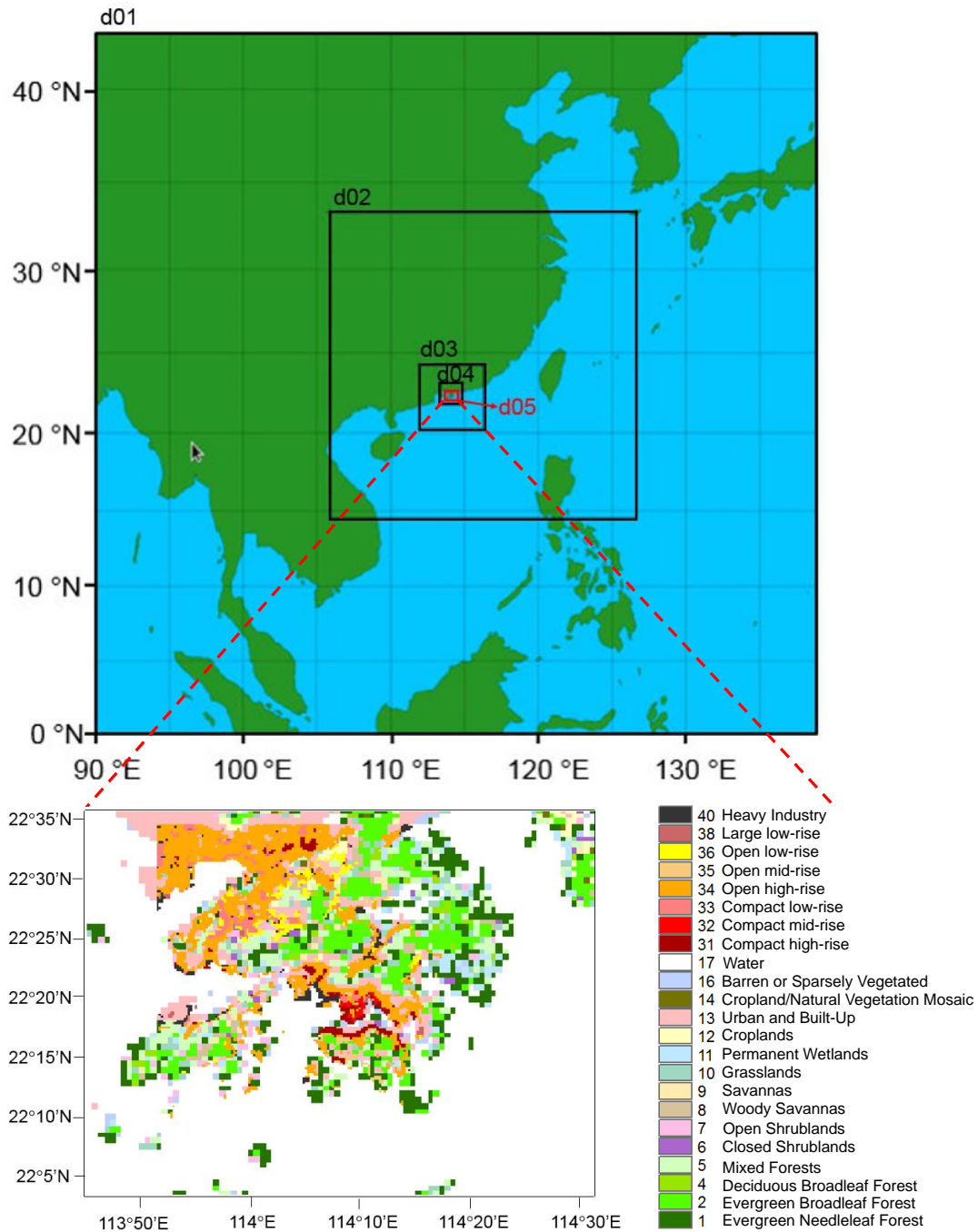


Figure 2. Domains in numerical model and LULC map for Hong Kong.

Table 1. Physical parameterizations considered in the WRF model.

Physics Options	Scheme	References
Microphysics	Single-Moment 3-class	[37]
Short Wave Radiation	Dudhia	[38]
Long Wave Radiation	Rapid Radiative Transfer Model	[39]
Cumulus	Kain-Fritsch	[40]
Boundary Layer	BouLac	[41]
Land Surface	Noah	[42]
Surface Urban	BEP/BEM	[34, 35]

3. Model evaluation

The observation data at 10 weather stations (Figure 3, Table 2) over Hong Kong were collected and compared against WRF-WUDAPT simulation results. The root-mean-square errors (RMSEs) of 2-m air temperature (T_2), 2-m relative humidity (RH_2), 2-m specific humidity (q_2), and 10-m wind speed (W_{10}) at all 10 stations (Table 2) were within acceptable ranges [33, 43-46], showing reasonable accuracy of model simulations. Specifically, for air temperature, RMSEs at all stations (1.1-1.8 °C) were comparable with previous WRF studies [33, 43, 44]. For relative humidity and specific humidity, average RMSEs at urban stations were slightly larger than those at most suburban and rural stations, which are all in similar ranges (RH_2 : 7.2-11.9 %, q_2 : 1.3-2.3 g/kg) with previous WRF studies covering over 10 cities in China [33, 44, 45]. For wind speed, RMSEs at urban and suburban sites are all lower than 2 m/s (benchmark set by US EPA [46]) except for relatively higher values at rural sites.

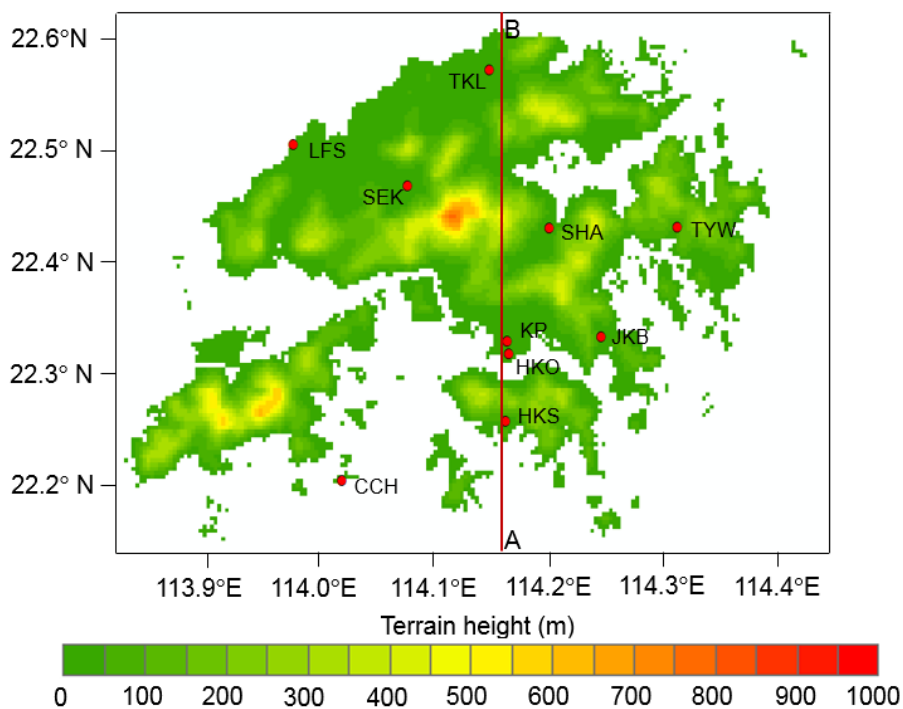


Figure 3. Location of weather stations over Hong Kong with the transect A-B crossing different LCZs.

Table 2. Ten weather stations and root-mean-square errors (RMSEs) between predicted and observed values for $T2$, $RH2$, $q2$, and $W10$ at each station. More detailed information about these stations can be found at: <https://www.hko.gov.hk/en/cis/climahk.htm>

Station	Classification	LCZ type	RMSEs			
			$T2$ (°C)	$RH2$ (%)	$q2$ (g/kg)	$W10$ (m/s)
KP	urban	LCZ4	1.3	9.8	1.8	0.9
HKO	urban	LCZ1	1.3	9.5	2.3	1.0
SHA	suburban	LCZ6	1.2	9.1	2.0	0.9
HKS	suburban	LCZ5	1.3	7.8	1.3	1.3
JKB	suburban	LCZ4	1.3	8.5	1.6	1.0
LFS	suburban	LCZ4	1.1	10.4	1.8	1.6
SEK	suburban	LCZC	1.3	8.7	2.1	0.9
TKL	rural	LCZ6	1.3	11.9	1.8	0.9
CCH	rural	LCZ4	1.8	8.3	1.3	2.2
TYW	rural	LCZA	1.7	7.2	1.5	/

To better illustrate the model capability, we selected three representative weather stations including HKO (urban), SHA (suburban) and TKL (rural), and showed the diurnal profiles of model-predicted values and observed values of $T2$, $RH2$, $q2$, and $W10$ at the three stations (Figure 4). Overall, the model is robust in replicating observed values with reasonable accuracy at all sites, except for some discrepancies possibly due to the uncertainties raised by differences between model and data resolutions during the model interpolation processes and relatively simple representation of moisture sources in the current WRF-BEP/BEM model. The peak temperature (Fig. 4a) was overpredicted and the peak wind speed (Fig. 4c) was slightly underpredicted especially at the urban site (HKO site). The possible reason is the discrepancy between model resolution (WRF grid: 333 m) and data resolution (LCZ map: 100 m) in the innermost domain and the associated uncertainties during the model interpolation processes using most-frequent LCZ types. For instance, the model grid (333x333 m²) encompassing a point-scale urban weather station was identified as open high-rise areas (LCZ4), while the weather station was actually sited at sparsely built areas (LCZ9). In addition, relative humidity (Fig. 4b) and specific humidity (Fig. 4d) at all sites were slightly underpredicted due to the absence of a realistic tree module and an effective anthropogenic moisture module in the current WRF-urban platform, which needs further exploration in the urban research community.

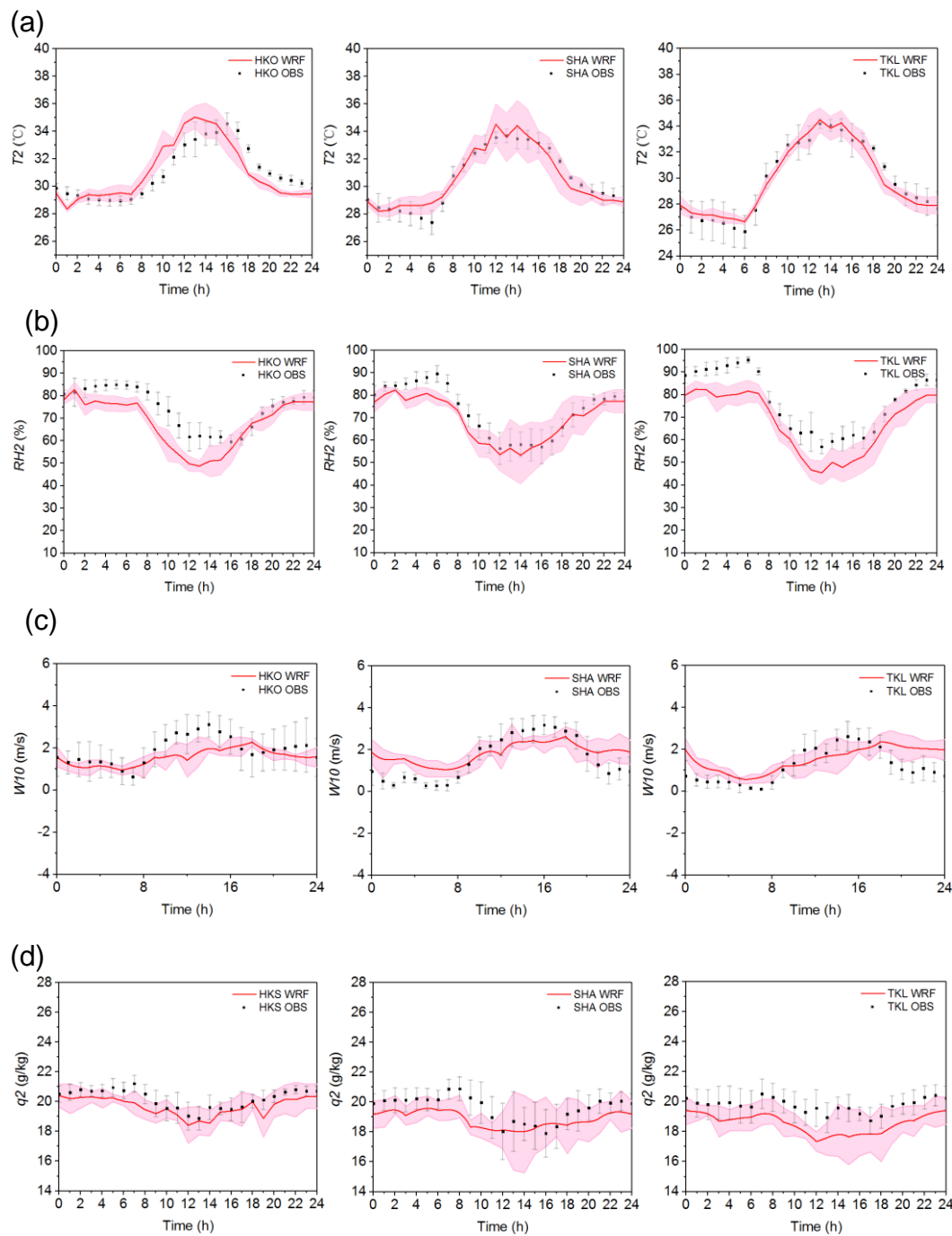


Figure 4. Comparison of model-predicted results against observed values for average diurnal cycle ± 1 standard deviation of (a) 2-m air temperature (T_2), (b) 2-m relative humidity (RH_2), (c) 10-m wind speed (W_{10}) and (d) 2-m specific humidity (q_2) at HKO, SHA and TKL sites.

4. Results and discussion

To quantify UHI and UMI, we first selected a representative rural reference site, i.e. TKL (Figure 3), which has been validated and applied extensively in previous urban climates studies [22, 47], and then calculated the urban-rural difference of 2-m air temperature (ΔT_2) and 2-m specific humidity (Δq_2), respectively over Hong Kong. If ΔT_2 and Δq_2 are positive, UHI and UMI occur, otherwise, urban cool island (UCI) and urban dry island (UDI) occur. In the following sections, we first presented the spatiotemporal variations of UHI and UMI intensities, and then studied the impact of sea breezes, mountain barriers and land-atmosphere interactions on the regional-scale and intra-urban moisture transport. Finally, we discussed the aggravated impact of concurrent UMI and UHI on thermal stress.

4.1 Spatiotemporal variation

Figure 5a shows the diurnal variation of the ensemble-averaged 2-m specific humidity for each LCZ type in Hong Kong, with peak values occurring near midnight. Figure 5b shows the diurnal variation of the ensemble-averaged Δq_2 , from which different characteristics of UMI and UDI effects can be identified. The UMI effect tends to occur at nighttime in compact high-rise and midrise areas (LCZ1&2) with the maximum intensity of 0.98 g/kg at 03:00 LT and at both daytime and nighttime in open low-rise, large low-rise as well as heavy industry areas (LCZ5&8&10) with a diurnally averaged intensity of 0.65 g/kg. The UDI effect tends to occur at the daytime (08:00-14:00LT) in compact high-rise and midrise areas (LCZ1&2) and at nighttime (20:00-02:00LT) in compact low-rise, open high-rise and open low-rise areas (LCZ3&4&6). Both UMI and

UDI effects were found to be non-significant in LCZ3&4&6 with small fluctuations of Δq_2 ranging from -0.5 to 0.5 g/kg except for open high-rise areas (LCZ4) at noon.

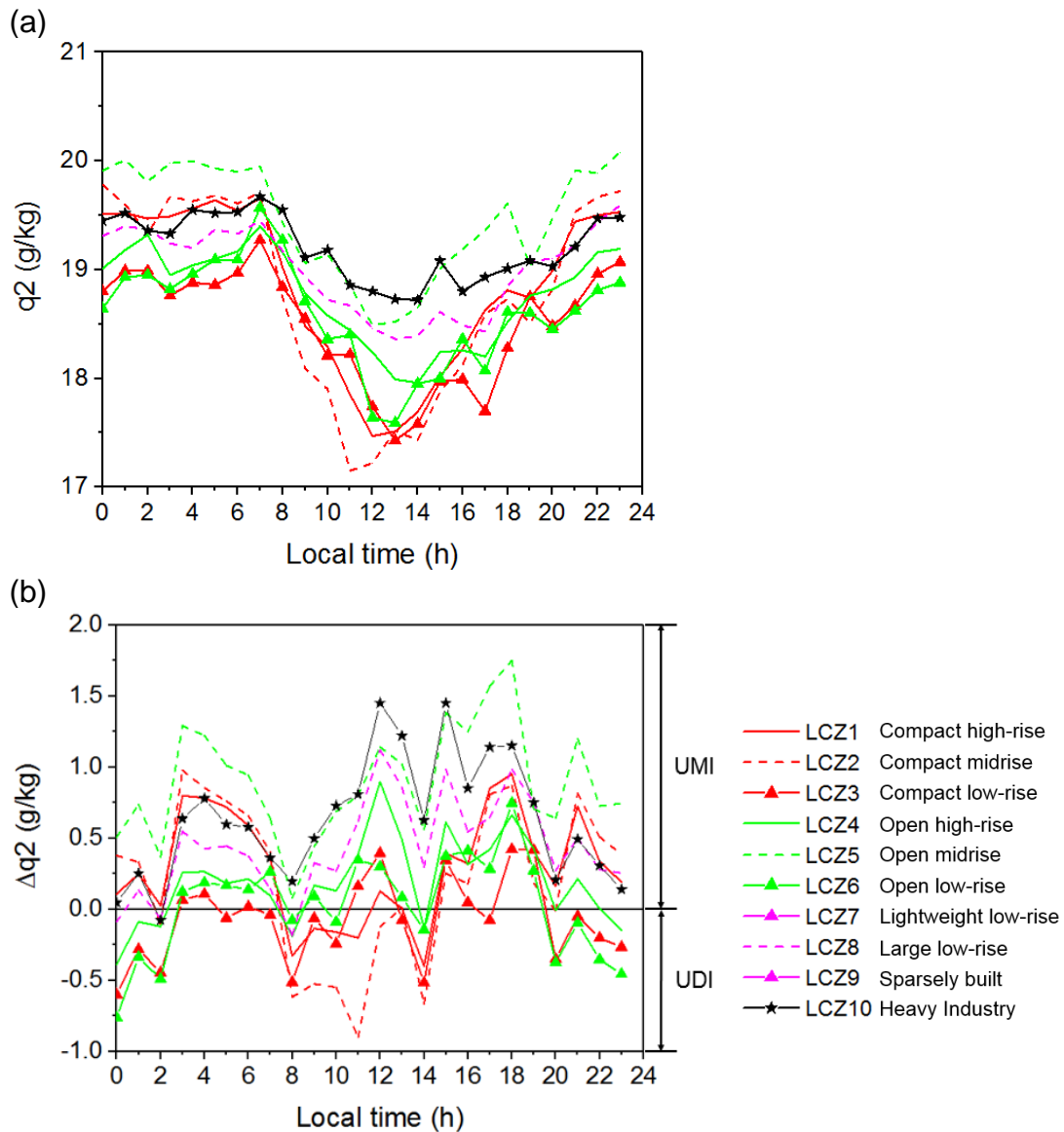


Figure 5. Diurnal variation of the ensemble-averaged (a) 2-m specific humidity, q_2 , and (b) urban-rural difference, Δq_2 for each local climate zone (LCZ) type.

Figure 6a shows the diurnal variation of the ensemble-averaged 2-m air

temperature for each LCZ type in Hong Kong, with peak values occurring in the early afternoon (13:00 or 14:00 LT). Figure 6b shows the diurnal variation of the ensemble-averaged ΔT_2 , from which different characteristics of UHI and UCI effects can be identified. The all-day UHI effect tends to occur in compact high-rise and midrise areas (LCZ1&2) with the maximum intensity of 3 °C and in compact low-rise, open high-rise, open low-rise areas as well as large low-rise areas (LCZ3&4&6&8) with a diurnally averaged intensity of 2.2 °C. By contrast, the UHI effects were found to be non-significant at nighttime in coastal areas (LCZ5&10) with small fluctuations of ΔT_2 ranging from 0 to 1.5 °C. The UCI effect tends to occur at daytime and in the early evening in open low-rise areas (LCZ5) (08:00-22:00LT) and heavy industry areas (LCZ10) (10:00-18:00 LT).

In addition, it is worth noting that, as shown in Figure 6, the T_2 had a considerable increase (about 1.1 °C) in compact areas at 01:00 LT, while an insignificant change (about 0.5 °C) in open areas and continuous decrease in natural surface areas. The rebounding at 0100LT in urban areas can be attributed to the higher anthropogenic heating efficiency than the longwave radiative cooling efficiency. During the earlier nighttime (1800LT-0100LT), the T_2 and ΔT_2 (Fig. 6) in urban areas had a continuous decrease due to cooling effect caused by upward longwave radiation. However, from 0100LT to 0300LT (in the dotted box), the anthropogenic heat in urban areas dominated the surface energy budget and caused the increase of T_2 and ΔT_2 , which delayed the cooling processes, especially in compact areas (LCZ 1&2&3) with the enhanced anthropogenic heat emissions. On the other hand, after 0300LT, the longwave radiative cooling effect at night dominated the surface energy budget

again and T_2 had a gentle decrease before sunrise (0600LT).

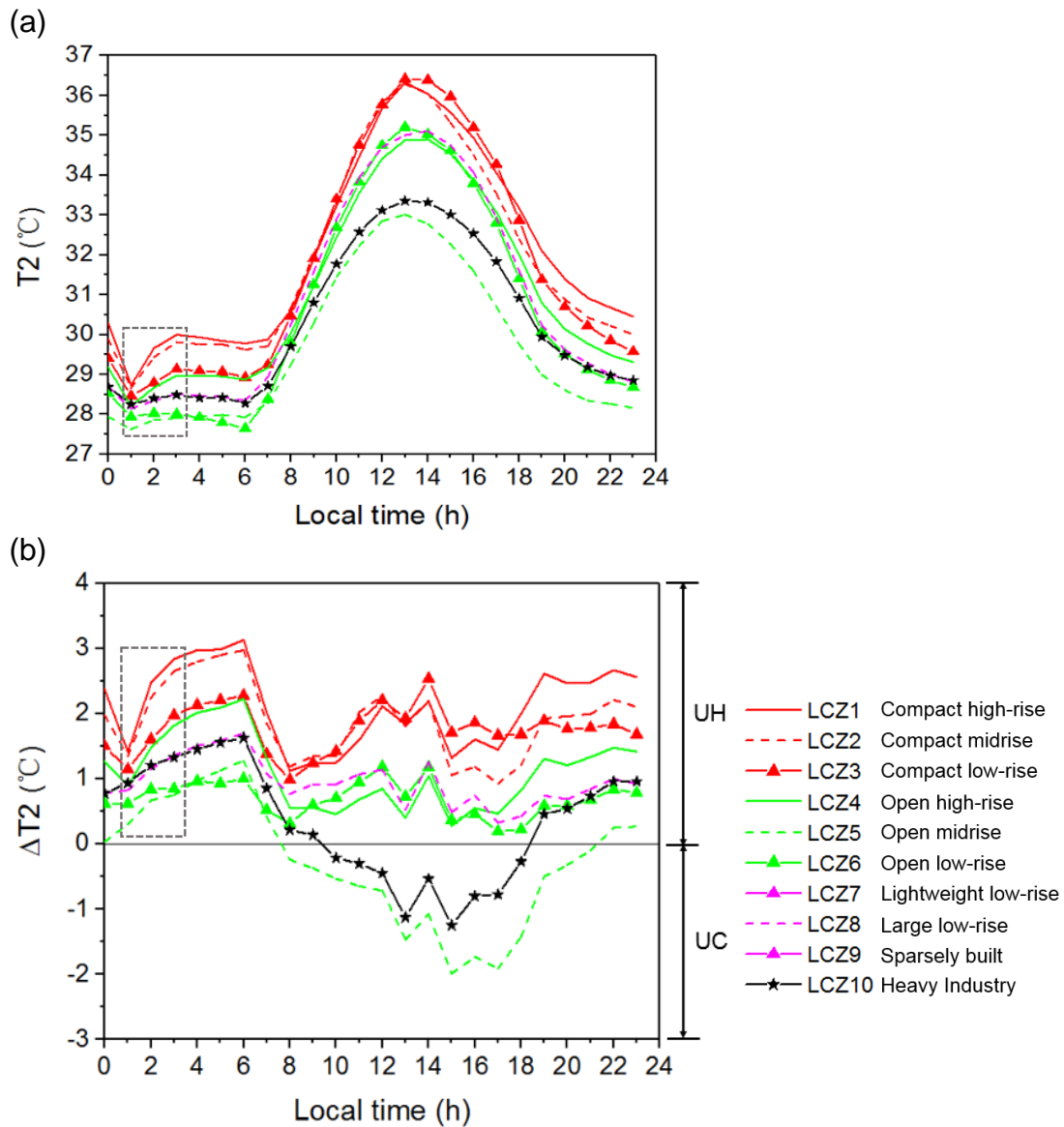


Figure 6. Diurnal variation of the ensemble-averaged (a) 2-m air temperature, T_2 , and (b) urban-rural difference, ΔT_2 for each local climate zone (LCZ) type.

4.2 Regional moisture transport

In this section, we investigated the regional moisture transport mechanism considering the impact of sea breeze and mountainous terrain. As shown in

Figure 5 and Figure 6, relatively high all-day UMI intensities and relatively high daytime UCI intensities were observed in open low-rise, large low-rise as well as heavy industry areas (LCZ5&8&10) and LCZ5&10, respectively, where most parts are in the coastal areas. The cool and humid sea breeze developed by the synoptic background wind could be important to the UMI and UCI effect in LCZ5&8&10. Figure 7 illustrates spatial distributions of UMI and UHI intensity over Hong Kong upon the background of wind fields at 04:00 LT and 14:00 LT. The synoptic wind direction was characterized by the prevalence of the southerly and from the sea toward the coast under the effect of the prevailing wind. The southerly sea breeze developed under background synoptic wind dominated inland areas for most of the time in a diurnal cycle and could penetrate to the north edge of Hong Kong, which was also reported by Lu et al. [48]. Meanwhile, compared to the onshore air, the marine air mass was characterized by the higher water vapor ratio at the daytime and nighttime (the sea-land difference was around 3.5 g/kg) and lower temperature at daytime (the sea-land difference was around -5 °C). Therefore, the incursion of this sea breeze could significantly humidify and cool the onshore air. Compared to inland areas, the coastal areas (e.g. most parts of open low-rise, large low-rise and heavy industry areas, LCZ5&8&10, see Figure 1) got priority in the displacement of hot and dry onshore air by moist and cool marine air.

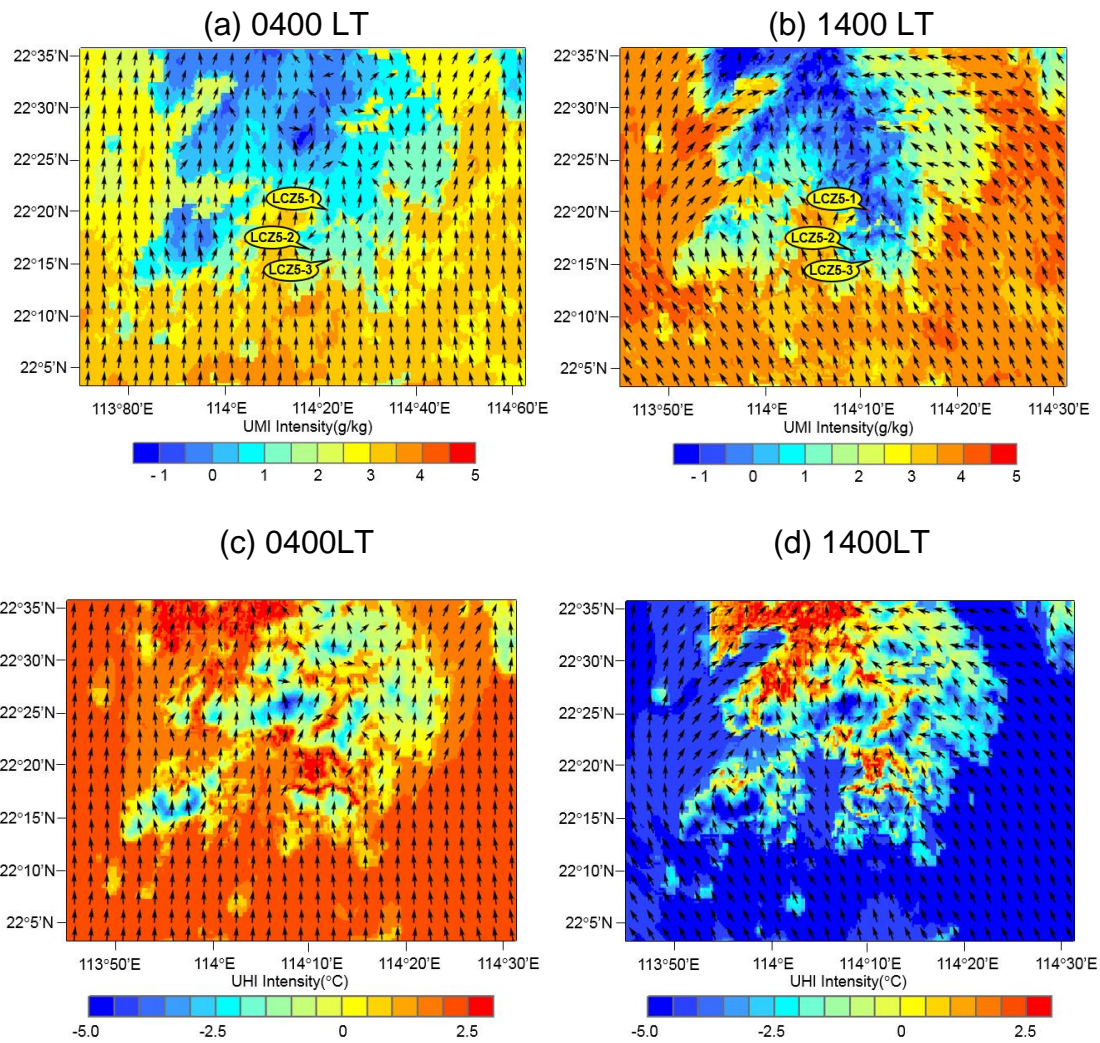


Figure 7. Ensemble mean of urban moisture island (UMI) intensities at (a) 04:00 LT and (b) and urban heat island (UHI) intensities at 14:00 LT; (c) 04:00 LT and (d) 14:00 LT. The vector is 10-m wind field at the same time.

Another important factor causing the decreased moisture in inland areas is the mountainous terrain of Hong Kong. Although the southerly marine air inflow penetrated further and dominated the entire mountainous land area, the 2-m specific humidity had a significant reduction along the south-to-north pathway at nighttime (Figure 7a&b). For example, the UMI intensities in three different regions of open low-rise areas (LCZ5) (LCZ5-1: 0.34 g/kg, LCZ5-2: 0.70 g/kg

and LCZ5-3: 1.19 g/kg) were found to be decreased with increasing distances to the coastline. To better examine the topographical effect on regional moisture transport processes, we selected a transect A-B (Figure 3) which crosses over most LCZ types and plotted water vapor and wind fields of the vertical cross-section along this transect in Figure 8. As shown in Figure 8 a&b, the water vapor ratio in the leeside of mountains was usually smaller than that in the upstream wind, possibly owing to the mountain barrier effects on the southerly sea breeze. As the moist flow had a stagnation due to upstream blocking effect of mountains, a relatively limited amount of moisture was able to reach the downstream regions [49, 50]. To evaluate the barrier effects of mountains on the water vapor, the drying ratio (*DR*) [51] can be obtained by :

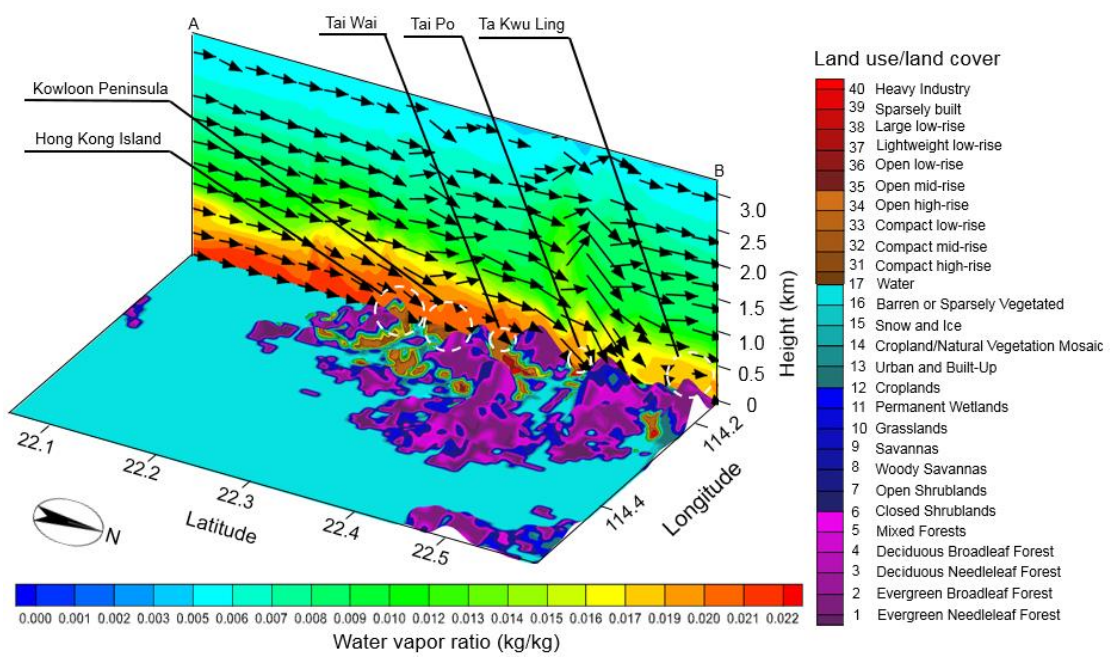
$$DR = \frac{F_{upstream} - F_{downstream}}{F_{upstream}} \quad (4.1)$$

where $F_{upstream}$ (g/kg) and $F_{downstream}$ (g/kg) are the water vapor ratio of the upstream and downstream wind, respectively. The *DR* of each mountain on the transect A-B ranged from 2.93% to 12.80% in the whole day, with an average value of 6.56%. There are four mountains along the transect A-B, which caused a maximum reduction of 23.83% in the water vapor ratio during the inland penetration of sea breeze.

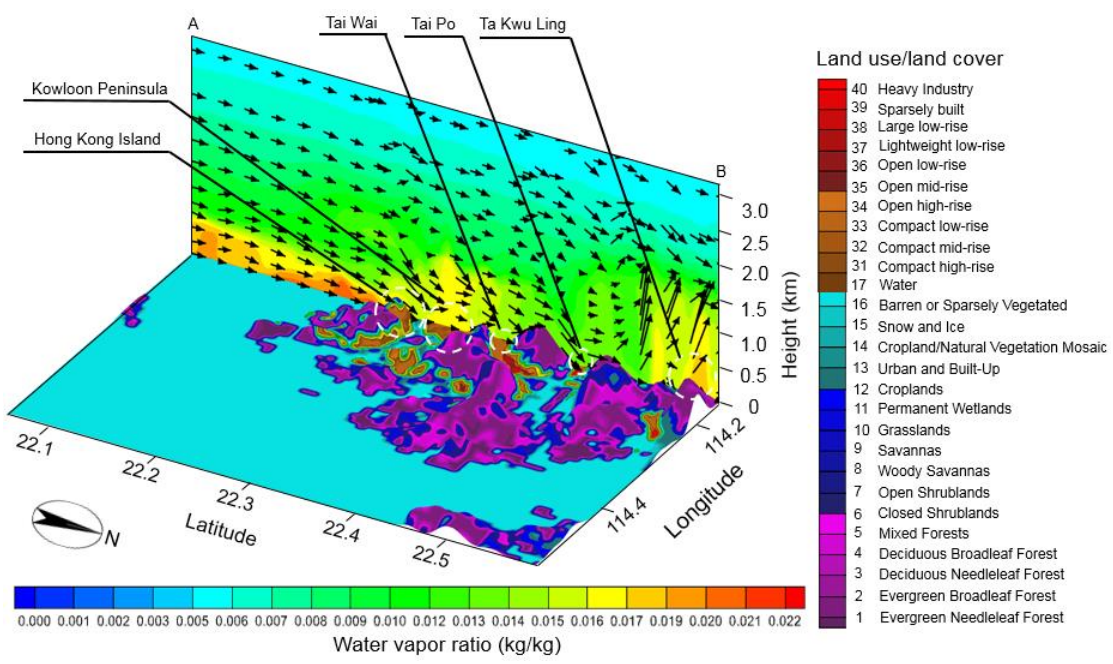
The mountain barrier had significant impacts at nighttime, while insignificant impacts at daytime on the 2-m specific humidity. As shown in Figure 7, nocturnal UMI and daytime UDI were observed in compact high-rise and midrise areas (LCZ1&2), where most parts are in the coastal areas. Although the mountain barrier can cause an all-day decrease of water vapor in the

downstream boundary layer, the vegetation evapotranspiration can replenish the depleted near-surface moisture at daytime. As shown in Figure 9, at nighttime, the 2-m specific humidity decreased considerably in the downstream flow of mountains due to the mountain barrier effect. However, at daytime, the 2-m specific humidity had a slight reduction in the upslope flow, and rebounded in the downslope flow due to the vegetation evapotranspiration. As a result, the 2-m specific humidity increased with fluctuations at daytime in the area between 22.37°N to 22.60°N, where most lands are covered by vegetation. The nocturnal decrease and daytime increase of 2-m specific humidity along the south-to-north pathway caused the nocturnal UMI and daytime UDI phenomenon in coastal areas (Figure 9), especially for the north Hong Kong Island and the Kowloon Peninsula (e.g. most parts of compact high-rise and midrise areas, LCZ1&2).

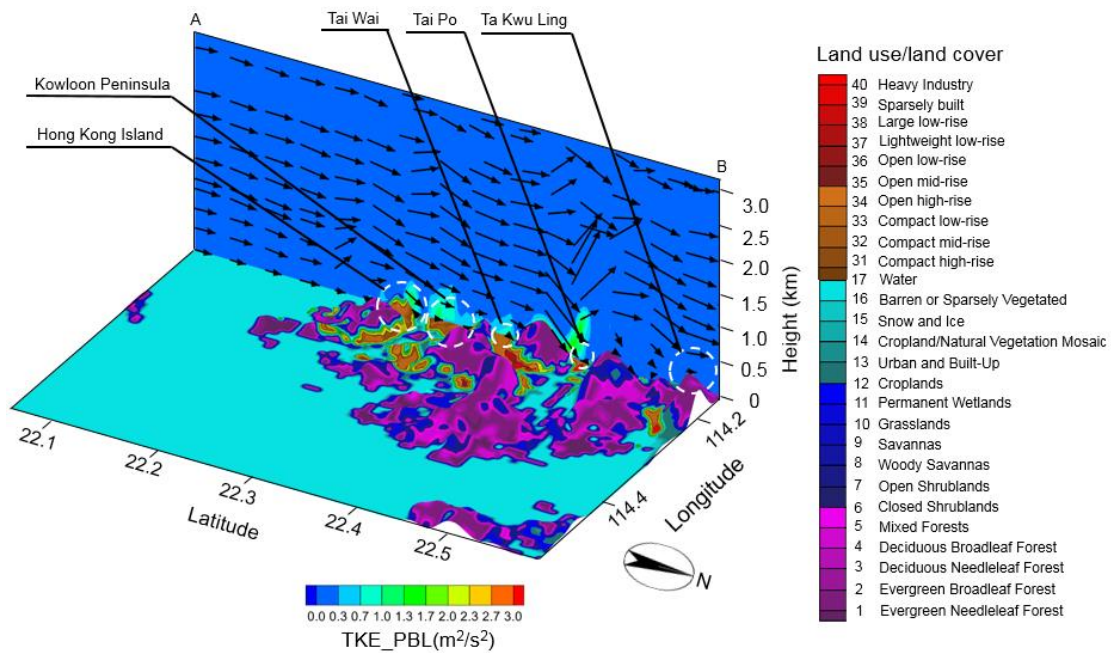
(a) 0400LT



(b) 1400LT



(c) 0400LT



(d) 1400LT

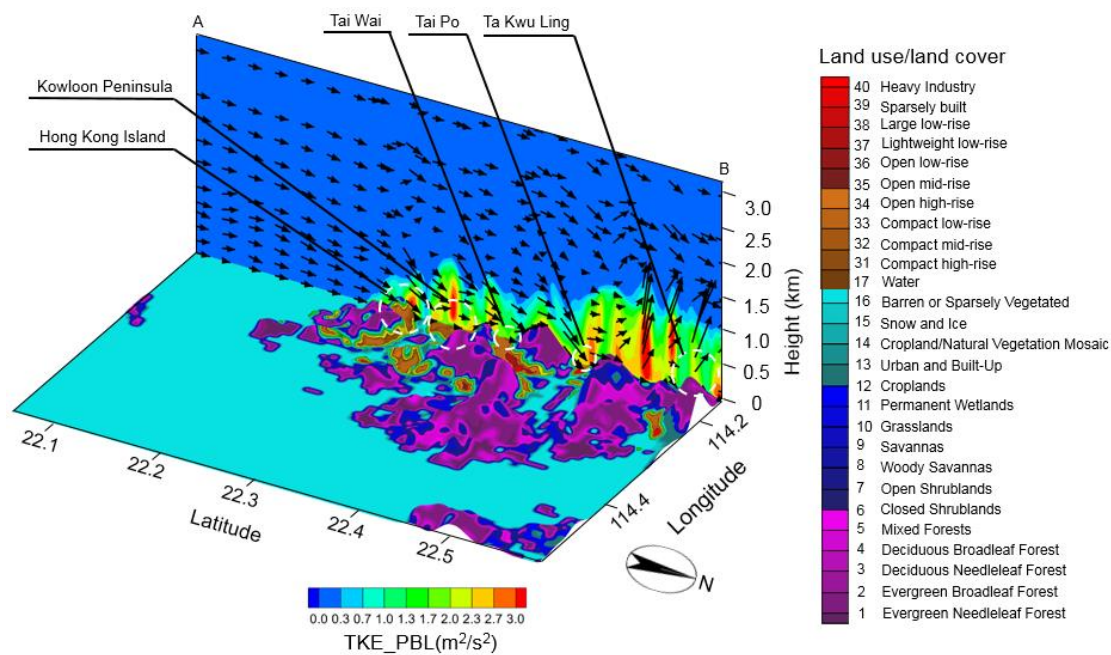


Figure 8. Vertical south-north cross section (transect A–B, shown in Figure 3) of the WRF-BEP/BEM model simulated vertical velocity (m/s) (vector) and water maxing ratio (g/kg) (contour on the slide) above ground level up to 3 km and the land use type (contour on the surface) at (a) 04:00 LT and (b) 14:00 LT;

and TEK_PBL (m^2/s^2) (contour on the slide) above ground level up to 3 km at (c) 04:00 LT and (d) 14:00 LT. The LULC level 31-40 are corresponding to local climate zones (LCZ) 1-10.

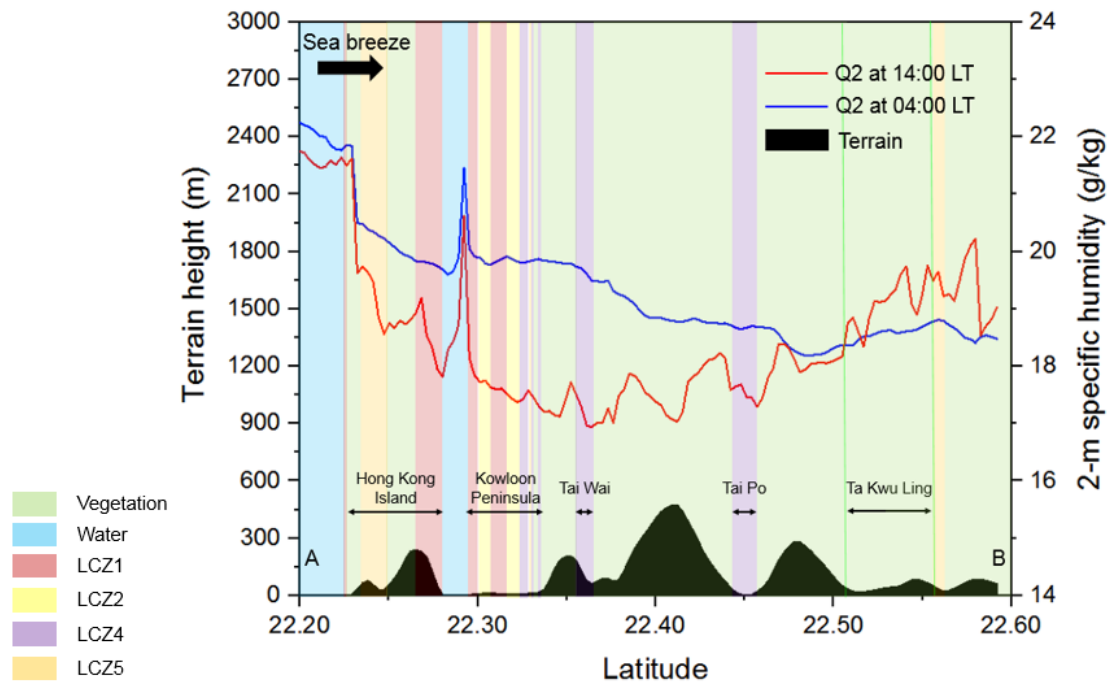


Figure 9. The ensemble-averaged 2-m specific humidity, ensemble-averaged 10-m wind speed and terrain height on the transect A-B.

The previous research [52] reported that UHI and UMI intensities tend to decrease with the increase of LCZ grades based on analysis of point-scale observation data with simplified regional impacts, while our results showed that UMI intensity did not monotonically decrease as the LCZ grades increased if more regional factors such as urban area location, sea breeze and terrain were considered in the mechanism analysis of UMI. The location of various LCZ areas, moist sea breeze, and mountain barrier effects were also important to local UMI intensities.

4.3 Urban moisture transport

In this section, we investigated the local moisture transport in urban areas considering the land-atmosphere interaction. The surface energy and moisture partitioning may differ in various LCZ types with the different urban morphology and physical parameters, which contributes to the special heterogeneity of air temperature and moisture contents. The thermal driven flow induced by the UHI effect could strongly modulate local moisture convection [53]. To better analyze the mechanism of UMI and UDI in urban areas, urban heat transport is first elaborated in this section. As shown in Figure 6, the UHI intensities closely followed the LCZ features. The street canyons could trap heat and weaken horizontal wind, which restricted the heat loss in the urban areas and caused the UHI effect. In addition, anthropogenic heat, low specific capacity of building material and high thermal storage in urban areas also had a crucial effect on the extremely high UHI intensities in compact high-rise and midrise areas (LCZ1&2). Compared to the intensive UHI effect in LCZ1&2, the moderate UHI effect in compact low-rise, open high-rise, open low-rise areas and large low-rise areas (LCZ3&4&6&8) (Figure 6) were attributed to their less compact buildings and higher nature surface fraction.

The spatial heterogeneity of energy partitioning can be important to near-surface humidity field. As shown in Figure 10a, the UHI effect caused the elevated near-surface sensible heat flux (SH), which reduced the atmosphere stability and caused the deeper PBLH in urban areas than in rural areas (Figure 10b). At the daytime, the average PBLH in compact areas (LCZ1&2&3) (around 2000m) was nearly 200m higher than that in open areas (LCZ4&6) and around

600m higher than that in coastal areas (LCZ5&8&10). The higher PBLH could facilitate vertical air motion and convection, and enhance vertical dispersion of moisture [54, 55]. On the other hand, the high near-ground SH, as well as the convergence zone induced by the combined effect of urban heat island circulation and sea-land breeze circulation [33] could enhance air mixing over urban areas. As a result, a dome-shaped boundary layer will form, with strong moisture mixing over urban areas and poor moisture mixing over rural areas [56]. The dome-shaped effect can confine moisture in shallow atmospheric layers.

The concurrent upward motion and dome-shaped effect can be important to the UMI and UDI effect in compact high-rise and midrise areas (LCZ1&2) (UMI intensity: 0.98 g/kg, UDI intensity: -0.90 g/kg) and open high-rise areas (LCZ4) (UMI intensity: 0.89 g/kg, UDI intensity: -0.19 g/kg) (Figure 5). At daytime, as shown in Figure 8d, there was upward motion strengthened by the UHI effect and dome-shaped boundary layer with the high TKE_PBL value over urban areas. Although the dome-shaped effect was characterized by a high moisture content in shallow atmospheric layers (Figure 8b), the upward motion caused a decrease of moisture near the ground, and therefore, the 2-m specific humidity at daytime (Figure 9) had a sharp decrease over urban areas, especially for the north Hong Kong Island and the Kowloon Peninsula (e.g. most parts of compact high-rise and midrise areas, LCZ1&2). At nighttime, urban areas were characterized by weak upward motion (Figure 8c), which was less effective to remove near-surface moisture, and therefore, the 2-m specific humidity at nighttime kept a relatively high level in urban areas than in rural

areas (Figure 9). Comparing to the intensive UMI and UDI effects in coastal compact urban areas (LCZ1&2), the moderate UMI and UDI in Tai Wai and Tai Po (e.g. most parts of open high-rise areas, LCZ4) were attributed to the less moist sea breezes and weak upward moisture motion.

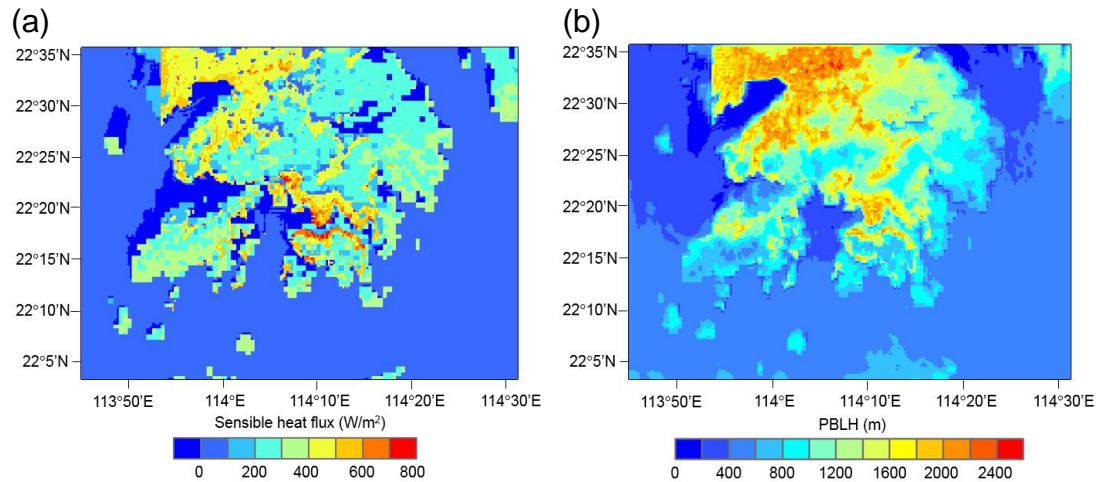


Figure 10. Ensemble mean of (a) surface sensible heat flux (SH) and (b) planetary boundary layer height (PBLH) at 14:00 LT.

Moreover, the significant UMI effect in compact high-rise and midrise areas (LCZ1&2) (Figure 5) at nighttime also corresponds to two other factors: weakened wind field and inhibited moisture condensation. As shown in Figure 11, comparing to the smooth incursion of sea breeze over other types of LCZ, the ventilation aisle in LCZ1&2 as blocked by the shielding effect of compact buildings, with converging surface winds. The weakened horizontal wind field was less effective to remove moisture and caused the UMI effect in LCZ1&2 at nighttime. In addition, the elevated temperature due to the UHI effect (Figure 6) during the heat wave event inhibited the dewfall and enhanced the near-surface specific humidity level in urban areas, which partly resulted in the UMI effect.

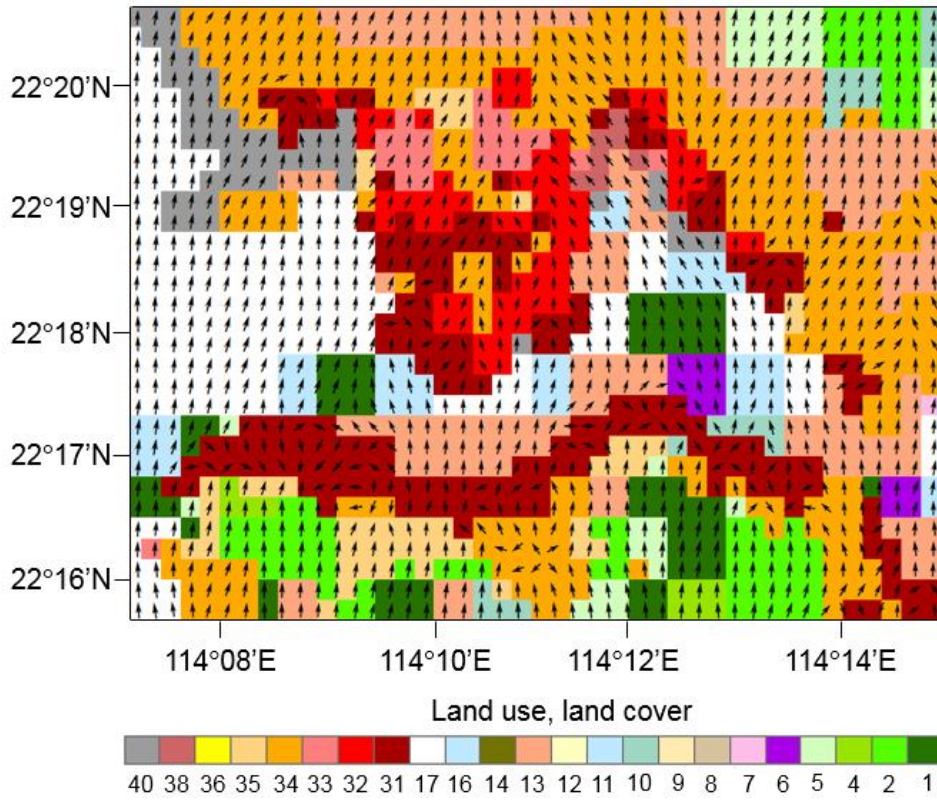


Figure 11. Ensemble mean of wind vector at 04:00 LT. The detail information of land use, land cover (LULC) is given in Figure 2. LCZ1 corresponds to LULC 31 and LCZ2 corresponds to LULC 32.

4.4 Implication on thermal comfort

In this section, we investigated the implication of UMI on thermal stress. To evaluate the heat risks associated with UHI and UMI effects, the heat index (HI) [57] which combines air temperature and relative humidity was introduced:

$$\begin{aligned}
 HI = & -8.784695 + 1.61139411 \times T + 2.338549 \times RH - 0.14611605 \times T \times RH \\
 & - 1.2308094 \times 10^{-2} \times T^2 - 1.6424828 \times 10^{-2} \times RH^2 + 2.211732 \times 10^{-3} \times T^2 \\
 & \times RH + 7.2546 \times 10^{-4} \times T \times RH^2 - 3.582 \times 10^{-6} \times T^2 \times RH^2
 \end{aligned}
 \tag{4.2}$$

Where T ($^{\circ}\text{C}$) is ambient dry bulb temperature and RH (%) is relative humidity.

As shown in Table 3, the HI was calculated over Hong Kong for the moment with the highest temperature at the HKO site. If only UHI was considered in thermal comfort evaluation, there were 53.87% of areas suffering from Extreme caution heat stress and no place was predicted as the Danger or Extreme danger area. However, if the synergistic effect of UHI and UMI was considered, the additional 37.64% and 6.14% of neighborhoods suffered from Extreme caution and Danger heat stress, respectively. Results indicate that there would be a significant underprediction of heat stress without considering the UMI effect, which is consistent with the study by Aktas et al. [58], reporting that assessment only based on temperature may cause an underestimation of heat index by 5 °C in most land-use areas of Kuala Lumpur, an Asian tropical city.

Table 3 The fraction of areas for different thermal stress level considering the combine effect of urban heat island (UHI) and urban moisture island (UMI), and UHI only.

Thermal stress levels	UHI+UMI	UHI only
Extreme danger (≥ 54 °C)	0	0
Danger (41-54 °C)	6.14%	0
Extreme caution (32-41 °C)	91.51%	53.87%
Caution (26-32 °C)	2.35%	46.13%

The WRF simulation based on BEP/BEM model can consider the heat trap, weakened wind, material properties and anthropogenic heat in urban canyons. Therefore, the numerical results can have a better representation of thermal comfort in urban areas. Meanwhile, the high-resolution (100m) geography data and urban morphological information from LCZ data give a possibility to the neighborhood-scale prediction. As shown in Figure 12, based on the

neighborhood-scale thermal stress map with 333m resolution, citizens can obtain timely, comprehensive and detailed heat warning information for their specific living or working areas during extreme heat wave events.

It is noted that HI posits a human-perceived equivalent temperature, which is an important index indicating thermal feeling. To consider the impact of UMI on thermal comfort independently, the averaged differences between HI and 2-m air temperature were calculated for various LCZ types. As shown in Figure 13, the impact of UMI on human thermal stress was found to be dominant at daytime in coastal areas (LCZ5&8&10) (5.4 °C) due to the highest UMI intensity and at nighttime in compact areas (LCZ1&2) (6.6 °C) due to the highest UHI intensity which aggravated the UMI impact on thermal comfort.

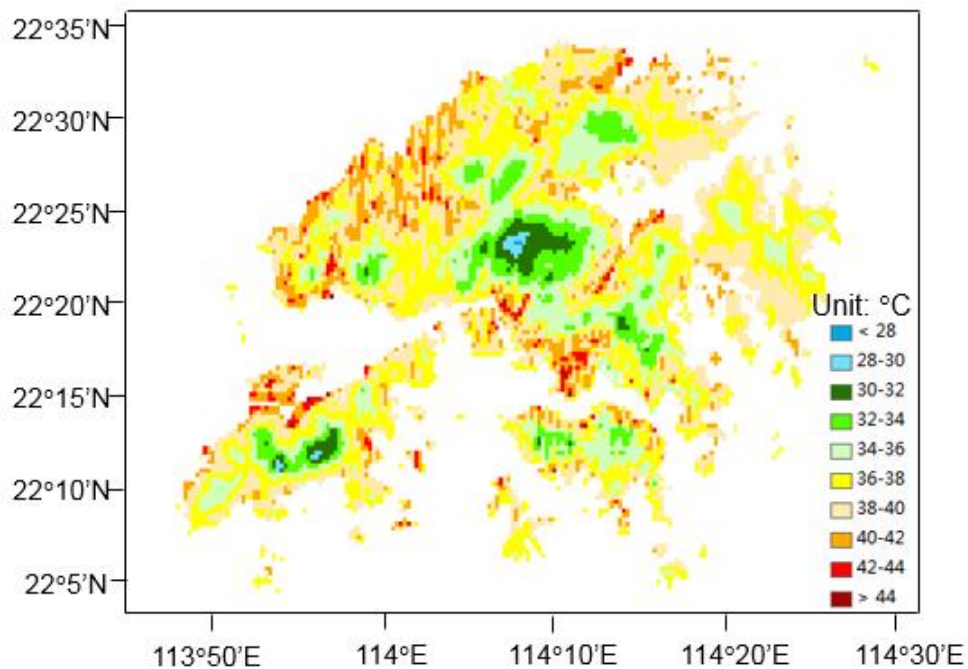


Figure 12. The simulated heat index over Hong Kong at 14:00 LT.

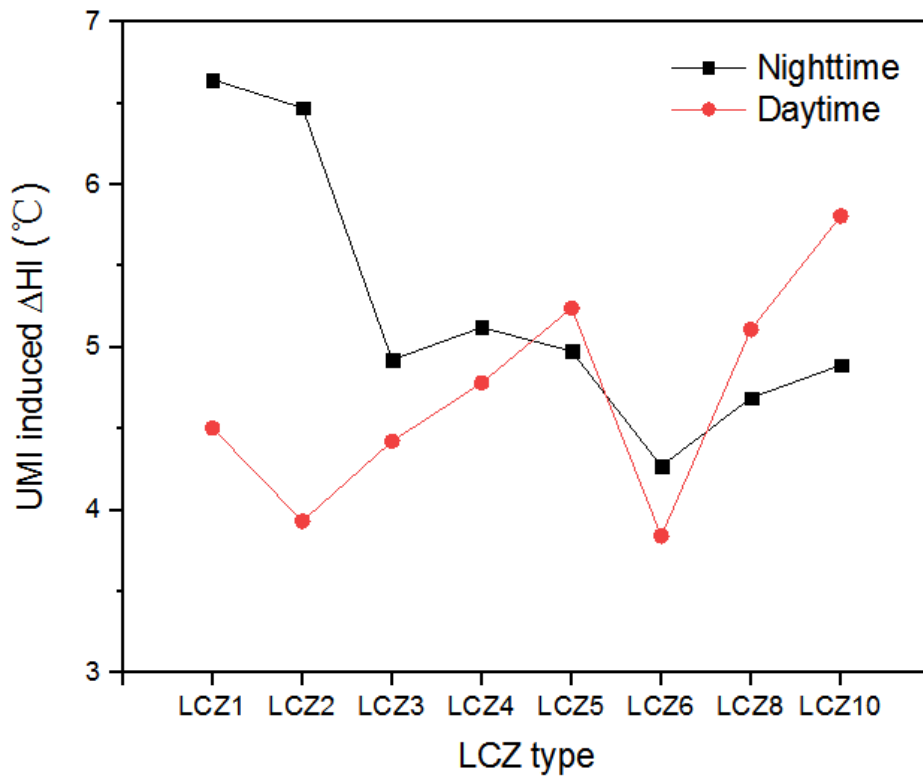


Figure 13. The averaged difference between heat index (HI) and 2-m air temperature for each LCZ type.

The present study hopefully provides useful guidance in adopting suitable UMI mitigation strategies for urban planners and policy makers. First, urban ventilation corridors should be unblocked for the smooth incursion of southern moist sea breeze and avoid moisture convergence zones, especially in coastal high-density high-rise areas. This can be achieved by planning broad north-south oriented street network in Hong Kong. Second, urban moisture sources such as building emissions and trees should be carefully controlled and planned via more informed strategies (e.g., optimal air-conditioning control and optimal tree species selection) especially in such compact high-rise cities [59]. Third, considering the heterogeneity of heat stress in space, the neighborhood-scale heat weather warning information should be published for citizens in different

city districts as a guidance to their plans of outdoor activities during hot and humid seasons.

5. Conclusion

In this study, we investigated the mechanism of the UMI effect and its implication on human thermal comfort over Hong Kong during a heat wave event (June 23-28, 2016) by employing a coupled WRF-BEP/BEM model with a high-resolution LCZ map based on WUDAPT methodology. Using this mesoscale model, the spatiotemporal UMI pattern, the regional/local moisture transport and the UMI implication on heat risks were studied for the first time. We found that at the regional scale, the UMI tends to occur in coastal areas, partly owing to the rich moisture source supplying by marine air inflow and inhibited moisture penetration due to mountain barrier effects. Specifically, a diurnal/nocturnal intensive UMI effect was found in coastal low-density areas (LCZ5&8&10) with an averaged intensity of 0.65 g/kg, while a nocturnal moderate UMI and a diurnal UDI were found in coastal high-density and midrise areas (LCZ1&2) with averaged intensities of 0.98 and -0.32 g/kg, respectively. The UDI effect was attributed to the increasing moisture upward motion induced by intensive near-surface SH in urban areas. The UMI effect at nighttime can be attributed to the weakened moisture convection, blocked ventilation corridors and inhibited dewfall associated with UHI.

In addition, the UMI effect had a tremendous impact on regional human thermal stress indicated by more portions of areas exposed to extreme heat risks, with 37.5% additional neighborhoods in Extreme caution level and additional 6.1%

neighborhoods in Danger level. Moreover, based on LCZ data, a high-resolution (333 m) neighborhood-scale map of heat index over Hong Kong was created, which can provide significant public health references for local residents and government planners. The map shows that UMI could significantly enhance human-perceived equivalent temperature, with the highest daytime increment in coastal low-density areas (LCZ5&8&10, 5.39 °C) due to the highest UMI intensity, while the highest nocturnal increment in compact high-density and midrise areas (LCZ1&2, 6.56 °C) due to the highest UHI intensities which aggravated the UMI impact on thermal comfort. Overall, this study gives a relatively comprehensive picture of UMI formation and its impact on heat stress. The current outcome is expected to be informative for city planners and stakeholders who are committed to mitigating the synergistic effect of UMI and UHI effects in coastal, subtropical and mountainous cities [60].

Acknowledgments

This work is supported by the Hong Kong Research Grants Council (RGC) Early Career Scheme Fund (Project number: 27208220) and General Research Fund (Project number: 17208021), HKU University Research Committee Seed fund for basic research for new staff, HKU Faculty of Engineering COVID-19 Action Seed Funding, and HKU start-up fund “Climate change prediction and adaptation for energy security and human health”. We also thank Dr. Chao Ren’s team at HKU for generating and sharing Hong Kong’s LCZ data.

References

- [1] S.J. Burian, J.M. Shepherd, Effect of urbanization on the diurnal rainfall pattern in Houston, *Hydrological Processes: An International Journal* 19(5) (2005) 1089-1103.
- [2] S.U. Grimmond, Urbanization and global environmental change: local effects of urban warming, *Geographical Journal* 173(1) (2007) 83-88.
- [3] K.W. Oleson, G.B. Bonan, J. Feddema, T. Jackson, An examination of urban heat island characteristics in a global climate model, *International Journal of Climatology* 31(12) (2011) 1848-1865.
- [4] T.R. Oke, The energetic basis of the urban heat island, *Quarterly Journal of the Royal Meteorological Society* 108(455) (1982) 1-24.
- [5] K. Lee, Y. Chan, T. Lee, W.B. Goggins, E.Y. Chan, The development of the Hong Kong Heat Index for enhancing the heat stress information service of the Hong Kong Observatory, *International journal of biometeorology* 60(7) (2016) 1029-1039.
- [6] E.L. Birch, S.M. Wachter, *Global urbanization*, University of Pennsylvania Press 2011.
- [7] S. Chapman, J.E. Watson, A. Salazar, M. Thatcher, C.A. McAlpine, The impact of urbanization and climate change on urban temperatures: a systematic review, *Landscape Ecology* 32(10) (2017) 1921-1935.
- [8] E.-J. Kim, H. Kim, Effect modification of individual- and regional-scale characteristics on heat wave-related mortality rates between 2009 and 2012 in Seoul, South Korea, *Science of The Total Environment* 595 (2017) 141-148.
- [9] C. Wang, S. Zhang, Y. Tian, B. Wang, S. Shen, Effects of simulated heat waves on ApoE^{-/-} mice, *International journal of environmental research and public health* 11(2) (2014) 1549-1556.
- [10] Y. Guo, A. Gasparri, B.G. Armstrong, B. Tawatsupa, A. Tobias, E. Lavigne, M.d.S.Z.S. Coelho, X. Pan, H. Kim, M. Hashizume, Heat wave and mortality: a multicountry, multicity study, *Environmental health perspectives* 125(8) (2017) 087006.
- [11] Z. Sun, C. Chen, M. Yan, W. Shi, J. Wang, J. Ban, Q. Sun, M.Z. He, T. Li, Heat wave characteristics, mortality and effect modification by temperature zones: a time-series study in 130 counties of China, *International Journal of Epidemiology* (2020).
- [12] B. Armstrong, F. Sera, A.M. Vicedo-Cabrera, R. Abrutzky, D.O. Åström, M.L. Bell, B.-Y. Chen, M. de Sousa Zanotti Stagliorio Coelho, P.M. Correa, T.N. Dang, The role of humidity in associations of high temperature with mortality: a multicountry, multicity study, *Environmental health perspectives* 127(9) (2019) 097007.
- [13] M. Geruso, D. Spears, Heat, humidity, and infant mortality in the developing world, *National Bureau of Economic Research*, 2018.
- [14] A.I. Barreca, Climate change, humidity, and mortality in the United States, *Journal of Environmental Economics and Management* 63(1) (2012) 19-34.
- [15] J. Zeng, X. Zhang, J. Yang, J. Bao, H. Xiang, K. Dear, Q. Liu, S. Lin, W.R. Lawrence, A. Lin, Humidity may modify the relationship between temperature and cardiovascular mortality in Zhejiang Province, China, *International journal of environmental research and public health* 14(11) (2017) 1383.
- [16] J.C. Lam, C. Tsang, D.H. Li, Long term ambient temperature analysis and energy use implications in Hong Kong, *Energy Conversion and Management* 45(3) (2004) 315-327.
- [17] W. Wang, W. Zhou, E.Y.Y. Ng, Y. Xu, Urban heat islands in Hong Kong: statistical modeling

and trend detection, *Natural Hazards* 83(2) (2016) 885-907.

[18] K. Hage, Urban-rural humidity differences, *Journal of Applied Meteorology and Climatology* 14(7) (1975) 1277-1283.

[19] W. Kuttler, S. Weber, J. Schonnefeld, A. Hesselschwerdt, Urban/rural atmospheric water vapour pressure differences and urban moisture excess in Krefeld, Germany, *International Journal of Climatology: A Journal of the Royal Meteorological Society* 27(14) (2007) 2005-2015.

[20] K. Richards, Urban and rural dewfall, surface moisture, and associated canopy-level air temperature and humidity measurements for Vancouver, Canada, *Boundary-Layer Meteorology* 114(1) (2005) 143-163.

[21] D.O. Lee, Urban—rural humidity differences in London, *International journal of climatology* 11(5) (1991) 577-582.

[22] Z. Wang, J. Song, P.W. Chan, Y. Li, The urban moisture island phenomenon and its mechanisms in a high-rise high-density city, *International Journal of Climatology* 41 (2021) E150-E170.

[23] R. Wang, C. Ren, Y. Xu, K.K.-L. Lau, Y. Shi, Mapping the local climate zones of urban areas by GIS-based and WUDAPT methods: A case study of Hong Kong, *Urban Climate* 24 (2018) 567-576.

[24] Y. Zheng, C. Ren, Y. Xu, R. Wang, J. Ho, K. Lau, E. Ng, GIS-based mapping of Local Climate Zone in the high-density city of Hong Kong, *Urban climate* 24 (2018) 419-448.

[25] Y. Wang, Y. Li, S. Di Sabatino, A. Martilli, P. Chan, Effects of anthropogenic heat due to air-conditioning systems on an extreme high temperature event in Hong Kong, *Environmental Research Letters* 13(3) (2018) 034015.

[26] J. Ching, G. Mills, B. Bechtel, L. See, J. Feddema, X. Wang, C. Ren, O. Brousse, A. Martilli, M. Neophytou, WUDAPT: An urban weather, climate, and environmental modeling infrastructure for the anthropocene, *Bulletin of the American Meteorological Society* 99(9) (2018) 1907-1924.

[27] I.D. Stewart, T.R. Oke, E.S. Kravynhoff, Evaluation of the 'local climate zone'scheme using temperature observations and model simulations, *International journal of climatology* 34(4) (2014) 1062-1080.

[28] O. Brousse, A. Martilli, M. Foley, G. Mills, B. Bechtel, WUDAPT, an efficient land use producing data tool for mesoscale models? Integration of urban LCZ in WRF over Madrid, *Urban Climate* 17 (2016) 116-134.

[29] M.A. Friedl, D.K. McIver, J.C. Hodges, X.Y. Zhang, D. Muchoney, A.H. Strahler, C.E. Woodcock, S. Gopal, A. Schneider, A. Cooper, Global land cover mapping from MODIS: algorithms and early results, *Remote sensing of Environment* 83(1-2) (2002) 287-302.

[30] A. Martilli, O. Brousse, J. Ching, Urbanized WRF modeling using WUDAPT, Technical Report March, Centro de Investigaciones Energeticas MedioAmbientales y Tecnologicas (CIEMAT), 2016.

[31] Hong Kong Observatory (HKO), The Weather of June 2016, (2016) <https://www.hko.gov.hk/en/wxinfo/pastwx/mws2016/mws201606.htm>.

[32] J.W.P. Tse, P.S. Yeung, J.C.-H. Fung, C. Ren, R. Wang, M.M.-F. Wong, C. Meng, Investigation of the meteorological effects of urbanization in recent decades: A case study of major cities in Pearl River Delta, *Urban climate* 26 (2018) 174-187.

[33] Y. Wang, S. Di Sabatino, A. Martilli, Y. Li, M. Wong, E. Gutiérrez, P. Chan, Impact of land surface heterogeneity on urban heat island circulation and sea-land breeze circulation in Hong Kong, *Journal of Geophysical Research: Atmospheres* 122(8) (2017) 4332-4352.

[34] A. Martilli, A. Clappier, M.W. Rotach, An urban surface exchange parameterisation for mesoscale models, *Boundary-layer meteorology* 104(2) (2002) 261-304.

- [35] F. Salamanca, A. Krpo, A. Martilli, A. Clappier, A new building energy model coupled with an urban canopy parameterization for urban climate simulations—part I. formulation, verification, and sensitivity analysis of the model, *Theoretical and applied climatology* 99(3) (2010) 331–344.
- [36] H. BEAM, Hong Kong Building Environmental Assessment Method, 2004.
- [37] S.-Y. Hong, J. Dudhia, S.-H. Chen, A revised approach to ice microphysical processes for the bulk parameterization of clouds and precipitation, *Monthly weather review* 132(1) (2004) 103–120.
- [38] J. Dudhia, Numerical study of convection observed during the winter monsoon experiment using a mesoscale two-dimensional model, *Journal of Atmospheric Sciences* 46(20) (1989) 3077–3107.
- [39] E.J. Mlawer, S.J. Taubman, P.D. Brown, M.J. Iacono, S.A. Clough, Radiative transfer for inhomogeneous atmospheres: RRTM, a validated correlated-k model for the longwave, *Journal of Geophysical Research: Atmospheres* 102(D14) (1997) 16663–16682.
- [40] J.S. Kain, J.M. Fritsch, A one-dimensional entraining/detraining plume model and its application in convective parameterization, *Journal of Atmospheric Sciences* 47(23) (1990) 2784–2802.
- [41] P. Bougeault, P. Lacarrere, Parameterization of orography-induced turbulence in a mesobeta-scale model, *Monthly weather review* 117(8) (1989) 1872–1890.
- [42] F. Chen, J. Dudhia, Coupling an advanced land surface–hydrology model with the Penn State–NCAR MM5 modeling system. Part I: Model implementation and sensitivity, *Monthly weather review* 129(4) (2001) 569–585.
- [43] M.-K. Hwang, J.-H. Bang, S. Kim, Y.-K. Kim, I. Oh, Estimation of thermal comfort felt by human exposed to extreme heat wave in a complex urban area using a WRF–MENEX model, *International journal of biometeorology* 63(7) (2019) 927–938.
- [44] Q. Wang, C. Zhang, C. Ren, J. Hang, Y. Li, Urban heat island circulations over the Beijing–Tianjin region under calm and fair conditions, *Building and Environment* 180 (2020) 107063.
- [45] I. Ribeiro, A. Martilli, M. Falls, A. Zonato, G. Villalba, Highly resolved WRF–BEP/BEM simulations over Barcelona urban area with LCZ, *Atmos Res* 248 (2021).
- [46] U.S. EPA, Guidance on the use of models and other analyses for demonstrating attainment of air quality goals for ozone, PM_{2.5}, and regional haze, United States Environment Protection Agency, Research Triangle Park, NC, 2007.
- [47] L.W. Siu, M.A. Hart, Quantifying urban heat island intensity in Hong Kong SAR, China, *Environmental monitoring and assessment* 185(5) (2013) 4383–4398.
- [48] X. Lu, K.C. Chow, T. Yao, J.C. Fung, A.K. Lau, Seasonal variation of the land–sea breeze circulation in the pearl river delta region, *Journal of Geophysical Research: Atmospheres* 114(D17) (2009).
- [49] D.J. Kirshbaum, B. Adler, N. Kalthoff, C. Barthlott, S. Serafin, Moist orographic convection: Physical mechanisms and links to surface–exchange processes, *Atmosphere* 9(3) (2018) 80.
- [50] Q. Jiang, Moist dynamics and orographic precipitation, *Tellus A: Dynamic Meteorology and Oceanography* 55(4) (2003) 301–316.
- [51] Smith, Ronald, B., Evans, Jason, P., Orographic Precipitation and Water Vapor Fractionation over the Southern Andes, *Journal of Hydrometeorology* (2007).
- [52] L. Shi, Z. Luo, W. Matthews, Z. Wang, Y. Li, J. Liu, Impacts of urban microclimate on summertime sensible and latent energy demand for cooling in residential buildings of Hong Kong, *Energy* 189 (2019) 116208.

- [53] J. Zhang, Y.-s. Zhou, X.-y. Shen, Numerical Simulation Analysis of the Impact of Urbanization on an Extreme Precipitation Event over Beijing–Tianjin–Hebei, China, *Atmosphere* 11(9) (2020) 945.
- [54] S.R. Davis, J.T. Farrar, R.A. Weller, H. Jiang, L.J. Pratt, The Land-Sea Breeze of the Red Sea: Observations, Simulations, and Relationships to Regional Moisture Transport, *Journal of Geophysical Research: Atmospheres* 124(24) (2019) 13803-13825.
- [55] R. Mahmood, R.A. Pielke Sr, K.G. Hubbard, D. Niyogi, P.A. Dirmeyer, C. McAlpine, A.M. Carleton, R. Hale, S. Gameda, A. Beltrán-Przekurat, Land cover changes and their biogeophysical effects on climate, *International journal of climatology* 34(4) (2014) 929-953.
- [56] H. Tong, A. Walton, J. Sang, J.C. Chan, Numerical simulation of the urban boundary layer over the complex terrain of Hong Kong, *Atmospheric environment* 39(19) (2005) 3549-3563.
- [57] L.P. Rothfusz, N.S.R. Headquarters, The heat index equation (or, more than you ever wanted to know about heat index), Fort Worth, Texas: National Oceanic and Atmospheric Administration, National Weather Service, Office of Meteorology 9023 (1990).
- [58] Y.D. Aktas, K. Wang, Y. Zhou, M. Othman, J. Stocker, M. Jackson, C. Hood, D. Carruthers, M.T. Latif, D. D'Ayala, Outdoor Thermal Comfort and Building Energy Use Potential in Different Land-Use Areas in Tropical Cities: Case of Kuala Lumpur, *Atmosphere* 11(6) (2020) 652.
- [59] X. Huang, J. Song, C. Wang, T.F.M. Chui, P.W. Chan, The synergistic effect of urban heat and moisture islands in a compact high-rise city, *Building and Environment* (2021) 108274.
- [60] Feng X., Chan T.O., Luo M., Different changes in dry and humid heat waves over China, *International Journal of Climatology*, 41(2) (2020) 1369-1382.